Water and Desalination Research Journal
Vol. 1, No. 1; 2017
Published by CanSRG
http://cansrg.com/journals/drj/

Effect of Natural Organic Matter on Scale reduction in Cooling Water Circuits: A Comprehensive assessment based on Empirical Characterization and Theoretical PHREEQCI Model computations

G.O Bosire[1,*] and J.C. Ngila[1,2]

[1] *Department of Applied Chemistry, University of Johannesburg, PO Box 17011, Doornfontein 2028 Johannesburg, South Africa*
[2] *Kenya Pipeline Company Morendat Institute of Oil &Gas, Kenpipe Plaza, Sekondi Road Off Nainyuki Road, Industrial Area, Nairobi, Kenya*

Abstract

This study examined a comprehensive semi-empirical approach assessing the influence of natural organic matter (NOM) on scale forming mineral phases in cooling water circuitry. Higher molecular weight NOM fractions were efficiently characterized and quantified using a combination of three techniques; viz the GC x GC-TOFMS (gas x gas chromatography with time-of-flight mass spectrometer) and LC-OCD (liquid chromatography-organic carbon detection) fluorescence emission excitation matrices (FEEM), the latter being a useful technique in confirming the type of humic substance in samples. Using the GC x GC-TOFMS, 80 low molecular weight organic compounds were determined in cooling water. The simulated scaling capacities due to interactions of metal ions and humics complemented experimental data favourably. Accurate speciation and simulative model computations were generated by the PHREEQC code, which suggested that Ca, Mg, Cu and Fe-based mineral phases potentially precipitate. Through unique speciation, complexation and saturation index profiles of these metals with fulvic acid in the modified Tipping and Hurley (T_H) database, their corresponding fulvate species such as CaFulvate, BaFulvate, MgFulvate, ZnFulvate, CuFulvate and FeFulvate+ were formed, which were found to influence saturation indices of mineral phases responsible for scaling in pipes.

Keywords: *Complexation; fulvate; speciation and simulative models.*

Nomenclature

ex	excitation
em	emission
EEM	excitation-emission map
dat	database
PHREEQCI	pH and redox equilibrium reactions interface
WHAM	Windermere's Humic Acid Model

Greek symbols

Φ	volume under an EEM
λ	wavelength

1. Introduction

For many years, natural organic matter (NOM) has been found to be ubiquitous in surface water. Generally, NOM is comprised of a range of compounds of higher molecular weight such as humic (HA) and fulvic acid (FA) [1] and lower molecular weight hydrophilic organic acids. These NOM components are known to play an important role in binding with metals to form stable complexes [2,3,4,5,6,7,8,9]. Most of the studies have focussed on NOM and its behaviour as a complex mixture of other compounds whose distribution gives it a distinct behaviour. As opposed to studying the behaviour of the NOM matrix, focussed studies on the behaviour of the individual

* Corresponding author
Submitted: September 11, 2017 Accepted: December 15, 2017

components in NOM are necessary. For example, recent studies have shown that humic acid and fulvic acid, which are the common compounds isolated from NOM, have distinctive chemical behaviour [10,11,12,13,14,15]. The individual characteristics of the various fraction influences speciation of metals, their chemical and biochemical interaction, bioavailability and environmental transport. In the first part of this study, we characterized and quantified NOM fractions of different molecular masses using relatively robust and fast analytical techniques. These techniques included the liquid chromatography-organic carbon detection (LC-OCD) [16,17], gas chromatography [18,19] and fluorescence techniques [20,21,22]. The second part is informed by the fact that, so far, the interactions of NOM fractions with metals can only be studied using the stability constants of metals in equilibrium with them. Therefore, the use of versatile computer codes with comprehensive or adjustable databases provided information on metal-NOM complexes. This approach is complementary to experimental inferences which may be expensive and time consuming.

Typical PHREEQC code simulations, for example, provide substantial models that can add value to experimental data [23,24,25,26]. It is worth noting that simulative models are reported in the literature [27,28,29,30,31]. Typical speciation calculations involve saturation indices and metal/ligand species in water. This study, for example, typifies a semi-empirical approach in two facets. In one way, the chromatographic/fluorescent determination specifies the NOM components available in the sample. In the second case, the versatile PHREEQC code databases can be adjusted to include equilibrium phases that reflect the chemistry of the specific metals with NOM fraction. If this can be done, then the metal-specific interactions with different fractions of NOM can be simulated.

The formation of stable complexes, in an aquatic environment, makes cations to remain in contact with DOC for tens of thousands of years. Consequently, long contact times between the elements in the aqueous phase and the DOM can be attained (over a range of physico-chemical parameters), and thereby minimizing any kinetic effects of complexation [32]. This long contact time presented us with the ability to assess the long-term partitioning of elements between the “free aquo-ion” and DOM phases.

The principal objectives of this work were; (i) to accurately characterize NOM in surface water used for cooling at Eskom power generation plants and (ii) to simulate complexation impacts on scaling potential by modifying and optimizing a conventional PHREEQC databases before running simulations. Modelling research, as observed in this study, could offer complementary simulations and speciation outputs that would ease the understanding of scale formation. Coupling of simulative modelling with characterization and quantification studies could provide a single, simple methodology for examining scale formation incidence in natural waters.

2. Materials and Methods

The concentrations of the metal ions were determined by inductively coupled plasma optical emission spectrometry (ICP-OES) (Spetro Arcos, with a Cetac ASX-520 auto-sampler) and the anions in the samples by ion chromatography, IC (ICS – 1500 model) using the Dionex IonPac^{TM} AS914 (Analytical 4 x 250 mm) column, and the Dionex IonPacTM AG14 (Guard 4 x 50 mm) column. The LC-OCD analyses were carried out on DOC-Labor LC-OCD instrument, Mode 8, Version 2012-08-27. The determination of NOM fractions (of <600 g molecular weight) in water preceding SPE extraction was performed using a using GC x GC gas chromatograph (Pegasus 4D, LECO Corporation, South Africa) with a time of flight mass spectrometer (TOF-MS). The

modelling software, PHREEQC, with an interactive interphase, was applied to generate speciation and saturation index simulation results.

2.1. Sampling and sample pre-treatment

Raw water samples from Vaal River were collected at the points feeding Lethabo and Kriel power stations, filtered through a 0.45 µm PES membrane and stored at 4ºC. Cooling water was collected at the various points in the cooling water processes pre-treated as done for raw water.

2.2. Materials and reagents

All reagents were of analytical grade unless otherwise stated, and Millipore water was used throughout the experiments. Solutions of nitric acid at concentrations of 0.1 mol L^{-1} used for pH adjustment were prepared from ultrapure concentrated acid (65%, Sigma-Aldrich, South Africa). Prior to ICP-OES analysis, the samples were acidified using nitric acid.

2.3. Instrumental analysis

The NOM fractions were characterized and quantified by the LC-OCD (DOC-Labor, Karlsruhe, Germany). Prior to LC-OCD-OND chromatographic separation, samples were passed through 0.45 µm filters and all the soluble organics were identified by the LC-OCD-OND system and the GC x GC-TOFMS.

2.3.1. Liquid chromatography-organic carbon detection (LC-OCD)

Dissolved organic matter (DOM) was subjected to a LC-OCD analysis. Using this technique DOM fractions, were separated into 5 different groups, all dependent on their molecular weights. That way, hydrophobic fractions, aromatic and molecular weights characteristic of aromatic hydrocarbons were assessed. A mobile phase was delivered with an HPLC pump (S-100, Knauer, Berlin, Germany) at a flow rate of 1.1 mL/min to an autosampler (MLE, Dresden, Germany, 1 mL injection volume) and the chromatographic column (a weak polymethacrylate cation exchange column (250 mm x 20 mm, TSK HW 50S, 3000 theoretical plates, Toso, Japan). Before chromatographic separations, water samples were passed through an in-built 0.45 µm PES membrane filters to remove particulate organic matter. This LC-OCD procedure was described in detail by Huber et al. (2011). The procedure also includes acidification of the water samples at the inlet of the OCD (at a flow rate of 0.2 mL/min) to convert carbonates to carbonic acid. This initial stripping process removes all inorganic carbon. Subsequent steps involve analysis of organic carbon, done by wet oxidation. Accordingly, the organic carbon detector (OCD) calibration was based on potassium hydrogen phthalate. In this case, the carbon mass was used to calibrate the OCD and its extinction coefficient, $\varepsilon = 1.683 \times 10^{-3}$ $Lmo1^{-l}cm^{-1}$ used to calibrate the UVD [16].

2.3.2. GC x GC-TOFMS

The GC technique employed the primary (RXi 5Sil-MS) and secondary dimension columns (RXi 17Sil-MS). The primary-dimension chromatographic separation column (5% 1,4-bis(dimethylsiloxyl)phenylene and 95% dimethylpolysiloxane) was 40 m long with internal diameter (ID) of 0.25 mm and 0.25 µm film thickness and the secondary dimension (x% phenyl, y% 1,4-bis(dimethylsiloxyl)phenylene and 50% dimethylpolysiloxane) column with an ID of 0.25 mm and the film thickness of 0.25 µm. The choice of the columns was based on the polarity and selectivity. The slightly polar RXi 5Sil-MS column incorporates phenyl groups in its polymer backbone, which improves its sensitivity, thermal stability, reduces bleeds and makes the

stationary phase less prone to oxidation. On the other hand, the RXi 17Sil-MS is intermediately polar and exhibits excellent inertness and selectivity for triglycerides, esters and phthalates. Nitrogen gas, compressed air and liquid nitrogen were used for quad-jet thermal modulator operation. The injector temperature for samples was set at 280 °C, at a volume of 1 µL on a split-less mode. Helium was used as the carrier gas at a flow-rate of 1.0 mL/min and a head pressure of 90 kPa. The modulator interface temperature was set at 30 °C above the secondary oven temperature. The transfer line temperature was set at 300 °C and the ion source temperature at 240 °C. Electron impact ionization energy was set at -70 eV with offset of 300 V totalling to the detector voltage of 1,600 V. The 1st dimension column temperature was started at 55 °C and held for 4.5 min, then increased to 280 °C at a ramping rate of 10 °C/min and held for 4.5 min; whereas, the secondary column temperature started at 75 °C held for 4.5 min then ramped to 310 °C at a ramping rate of 10 °C/ min and held for 4.5 min.

2.3.3. FEEM analysis

Fluorescence emission excitation matrices (FEEMs) were collected using a Horiba AquaLog Spectrometer (Jvon, New Jersey, USA). No pre-treatment of the samples was applied. Maintaining a common pH between samples ensures that the fluorescence characteristics of the acidic functional groups in humic molecules remain constant. For this reason, all the samples were adjusted to a pH of 7. Collection of intensity values at 10 nm increments within excitation-emission ranges of 250-450 nm and 300-600 nm, respectively. Scan rate was set to 600 nm/min, slit width was set to 10 nm and photomultiplier tube voltage was set to 775 V. Type 1 water at pH of 7 was used as a blank solution. The fluorescence spectrometer used a xenon lamp excitation source and the emission at longer wavelengths was detected at 0.3 nm steps. Further to this inner-filter correction and Rayleigh scattering was applied to the data.

Peaks at shorter excitation wavelengths (280 nm) and longer emission wavelengths (>380 nm) are associated with humic acid-like compounds. This DOM-related spectral information lacks capabilities of quantifying multiple broad-shaped EEM peaks. Chen et al (2003) postulated that integration beneath EEMs within selected regions would represent cumulative fluorescence responses of DOM with similar properties. This technique shows that the volume (Φ i) beneath a region said to be i of an EEM be calculated by the equation 1;

$$\Phi_{\mathrm{i}} = \int_{ex}^{x} \int_{em}^{x} I(\lambda_{ex}\lambda_{em}) d\lambda_{ex} d\lambda_{em} \quad (1)$$

where $d\lambda_{ex}$ is the excitation wavelength interval (taken as 10 nm), $d\lambda_{em}$ is the emission wavelength interval (taken as 0.5 nm), and $I(\lambda_{ex}\lambda_{em})$ is the fluorescence intensity at each excitation-emission wavelength pair. The values of Φ i can be normalized to a DOC concentration of 1 mg/L for comparison of EEMs from different sources of NOM [33].

2.3.4. Metal analysis

Water samples were filtered using 0.45 µm membrane filters. All sample volumes for trace element analysis were subsequently acidified with 0.1M HNO_3. ICP-OES measurements were done using a Thermo Fisher ICP instrument. The blanks were acidified Type 1 water. In addition, the trace metals (in ppb levels) were measured using the ICP-MS. All statistical computations were performed using the OriginLab version 8 software.

2.4. Geochemical modelling

A modified PHREEQC geochemical code, was used to calculate the aqueous speciation and saturation indices of different mineral phases. The humate and fulvate thermodynamic definitions were incorporated into a Tipping_Hurley with a WHAM database (T_H.DAT) [2]. Table 1 shows the log K values for equilibrium phase equations of the reactions incorporated into the T_H.DAT database together with their stability constants, all drawn from visual MINTEQ v 3.1.1. For these reactions, the phases were defined as SOLUTION_SPECIES in T_H.DAT. The modified T_H.DAT incorporated log K values from *risbergfa13.vdb, shmgeneric10.vdb, genericha08.nic and genericfa08.nic* databases in visual MINTEQ version 3.1. These values define the equilibrium phase equations of fulvic acid with Mg^{2+}, Ca^{2+}, Cu^{2+}, Zn^{2+}, Fe^{3+}, Ba^{2+} and Al^{3+} that give rise to corresponding fulvates.

Table 1. Equilibrium phase equations defined in T_H.DAT as SOLUTION_SPECIES using the NICA-Donnan visual MINTEQ [2]

Phase	Equilibrium reaction	Log K
#CaFulvate	Ca+2 + Fulvate-2 = CaFulvate	-3
#MgFulvate	Mg+2 + Fulvate-2 = MgFulvate	-2.4
#AlFulvate	Al+3 + Fulvate-2 = AlFulvate+	12.16
#BaFulvate	Ba+2 + Fulvate-2 = BaFulvate	-4.8
#ZnFulvate	Zn+2 + Fulvate-2 = ZnFulvate	-0.73
#CuFulvate	Cu+2 + Fulvate-2 = CuFulvate	8.26
#FeFulvate	Fe+3 + Fulvate-2 = FeFulvate	-1.1

The pH, alkalinity, metal cations and anions were modelled together with organic components (fulvates) using a fulvate adjusted T_H database. To show mineral dissolution or precipitation, saturation indices (SI) were calculated. Herein, a general reaction (equation 2), describes super-saturation which is the key parameter that determines precipitation. The saturation ratio (S) is described as the ratio of the ionic activity product (IAP) to the equilibrium constant (Ks) (equation 3).

$$A^- + B^+ = AB + g + l \quad (2)$$

where A^- is the anion being equilibrated ($A^- = CO_3^{2-}$, SO_4^{2-}, or PO_4^{3-}) B^+ is the metal cation, AB is the mineral phase formed and g and l are any gas or liquid phases respectively.

$$S = \frac{IAP}{K_s} = \frac{[A^-][B^+]}{K_s} \quad (3)$$

A value of S < 1, indicates an under-saturated solution, S = 1 shows a solution in equilibrium with the solid, while S > 1 shows a supersaturated solution, which leads to precipitation/scaling. Saturation indices (SI) are defined as SI = log10(S), so that an equilibrium situation corresponds to SI = 0, and under-saturation and super-saturation shown by SI < 0 and SI > 0, respectively.

3. Results and Discussion

The determination of scaling potential is very difficult because conventional analysis of water only gives the total concentrations of cations and anions, physicochemical characteristics and quantities of dissolved organic matter. However, scaling simulations could be achieved by computer codes that perform speciation and saturation index calculations. The results in this article present both

empirical and modelling studies based on a detailed assessment of main organic frations (>600 g molecular weight) in raw and cooling water at Lethabo using LC-OCD. Organic compounds with molecular weight >600 g (extracted by solid phase extraction), were determined by the 2-dimensional GC x GC-TOFMS.

3.1. Components of raw and cooling water

Table 2 shows results obtained for pH, conductivity, organic carbon and nitrogen, anions and common and trace cations. The raw and cooling water were alkaline with pH values ranging 8.91 to 10.46. It was also observed that the raw and cooling water in the cooling water circuit (CWC) had relatively higher levels of Ca and Mg among the metals analysed. The concentrations of these scale forming metals (Ca and Mg) ranged 7.5-158.2 and 15.6-236.0 mg/L throughout all the stages of the cooling water process. The sulphate concentrations were lowest in raw water but were 10 to 20-fold in the CWC. We attribute this to high scaling potential in the water pipes. The DOC levels in other stages of the CWC ranged 38.8 to 81.4 mg/L, which were distinctly 10-20-fold the values measured in raw water (4.0 to 5.9 mg/L). From the solubility of humic and fulvic fractions in DOC reported in literature, the pH interval reported in this study favours solubility of these important fractions.

Table 2. The composition and characteristics of raw and cooling water

Analyte (in ppm)	Lethabo Water				Kriel Water			
	Raw	*Clarified water*	*Inlet*	*Outlet*	*Raw*	*Clarified water*	*Inlet*	*Outlet*
pH	10.22	9.05	9.6	8.91	9.97	9.74	10.46	9.69
Conductivity	0.177	4.63	4.05	4.67	0.283	3.49	3.25	3.46
Common anions (IC)								
Fluoride	0.596	2.11	2.066	2.306	0.65	2.6	1.15	3.06
Bromide	ND	158.95	159.57	166.41	ND	47.42	43.85	41.75
Sulphate	0.0878	5.595	4.107	5.98	0.2	3.442	5.08	3.12
Common and trace cations (ICP-OES/MS)								
Ca[a]	7.85	34.53	38.94	37.81	11.25	142.95	154.6	158.2
Mg[a]	15.46	212.08	231.9	236.0	17.41	97.43	111.9	115.3
Ba[a]	0.0450	0.8982	0.1149	0.1190	0.0554	0.1312	0.2204	0.2331
Cu[b]	0.0082	0.0454	0.0477	0.0565	0.0105	0.1014	0.2187	0.2204
Fe[b]	0.0330	0.0122	0.01307	0.0154	0.2931	0.0158	0.0150	0.0159
Cr[b]	0.0055	0.0132	0.0135	0.0133	0.0053	0.0169	0.0227	0.0208
Zn[b]	0.0015	0.0002	0.0007	0.0027	0.0013	0.0025	0.0052	0.0028
Organic carbon and nitrogen (LC-OCD-OND)								
DOC (ppb)	4022	45902	25830	38775	5934	47023	49290	81422
DON (ppb)	292	2428	1543	1915	361	5457	3212	3224
HS(% DOC)	89.5	80.0	84.1	83.5	88.4	84.6	87.8	86.3
SUVA	5.34	3.29	3.78	3.28	4.58	3.23	3.78	3.82

[a] *Concentrations obtained by ICP-OES*
[b] *Concentrations obtained by ICP-MS*

Humic substances (HS) across our samples range of 80 to 90% of the DOC with the rest comprising mainly of low molecular weight compounds. Some of these low molecular compounds are determined by gas chromatography (Section 3.2). However, the percentage of HS in the raw water was higher than in CWC. This observation correlates very well with the specific UV absorbance at λ_{254} (SUVA) values. The highest SUVA values were observed in the raw water, regardless of

the power station (Table 2), indicating a relatively higher concentration of HS or hydrophobic compounds. To understand the differences in SUVA results, Section 3.3, gives an account of the changes that occur to raw water as a function of evaporative simulations. The removed portion of HS (considered high molecular weight), suggests degradative processes in the cooling towers because of relatively high temperatures (35-49 ˚C), which has an effect on the composition of NOM [34]. This possible explanation agrees with results presented later in this article on simulation discussions.

As observed, after clarification of the cooling water, the SUVA values decreased. This means that the clarifier process removes some HS responsible for high hydrophobicity. Coincidentally, the dissolved organic nitrogen levels were highest at the clarifier outlet, i.e. 2.4 (Lethabo) and 5.4 mg/L (Kriel). Based on these results, a further study on the effect of clarifier procedures on NOM composition, is still necessary.

3.2. GC x GC-TOFMS

Considering the results reported in the previous section, the low molecular weight compounds comprise 10% of DOC. These organic compounds were analysed by GC x GC-TOFMS and identified as straight chain aliphatic organics, aromatic organics, substituted aliphatic organics and alicyclic organics. The results revealed that a considerable portion of organics were aromatics, with a higher number being observed in CWC. The attention drawn to aromatic organics follows the fact that the degree of aromaticity helps to explain the hydrophobic nature of these compounds (explained in Section 3.3, under the HS-diagram). Eighty organic compounds were determined in the CWC and 63 in raw water. Selected compounds representing each class are shown in Table 3.

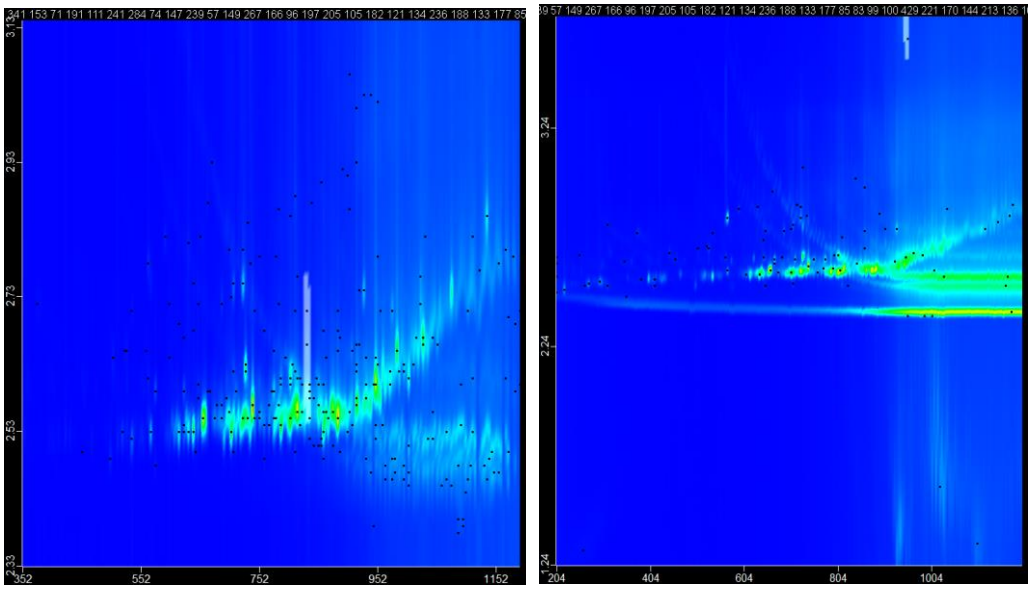

Figure 1: Two-dimensional chromatograms showing the total number of organic compounds of molecular weight <600 g extracted from raw (A) and cooling water obtained from Lethabo power generating station of Eskom, South Africa.

The chromatograms of raw and cooling water are presented in Figure 1. Using the Strata^{TM} X SPE and GC x GC-TOFMS with chromaTOF software, the organic compounds discriminated by 1st

Table 3. Selected low molecular weight organic compounds (MWt <600 g) identified in raw water and in the CWC by the GC x GC-TOFMS (R.T stands for retention time).

	RAW WATER			WATER IN CWC		
Classes of compounds	Names of compound	1D R.T (Sec)	2D R.T (Sec)	Name of compound	1D R.T (Sec)	2D R.T (Sec)
Aromatic hydrocarbons	Phenol, 2,4-bis(1,1-dimethylethyl)-	528	2.650	1,2-Benzenedicarboxylic acid, butyl 2-ethylhexyl ester	724	2.830
	Benzoic acid, 4-ethoxy-, ethyl ester	536	2.710	1,2-Benzenedicarboxylic acid, bis(2-methylpropyl) ester	688	2.770
	4-Ethylbenzoic acid, 3-fluorophenyl ester	732	2.840	Phenol, 2,2'-methylenebis[6-(1,1-dimethylethyl)-4-methyl-	892	2.850
Substituted compounds	Methyl tetradecanoate	788	2.600	Formamide, N,N-dimethyl-	204	2.560
	Isopropyl myristate	668	2.590	N,N-Dimethylacetamide	204	2.620
	Decane, 2,3,5,8-tetramethyl-	536	2.520	1-Dodecanol, 2-octyl-	1168	2.840
Cyclic compounds	(7-Isopropylidenebicyclo[2.2.1]hept-5-en-2-ylidene)acetonitrile	812	2.880	Cyclopropane, propyl-	952	2.380
	2,5-Cyclohexadiene-1,4-dione, 2,6-bis(1,1-dimethylethyl)-	504	2.640	Cyclopentaneundecanoic acid, methyl ester	712	2.640
	Cyclopentaneundecanoic acid	844	2.580	Cyclodocosane, ethyl-	924	2.630
Aliphatic compounds	Erucic acid	868	2.550	trans-13-Octadecenoic acid	1028	2.560
	trans-13-Octadecenoic acid	1068	2.530	n-Hexadecanoic acid	1160	2.520
	cis-7-Tetradecen-1-ol	708	2.620	n-Decanoic acid	456	2.640

and 2nd dimension retention times were identified as shown by the 2D-contour chromatograms. The chromaTOF software enabled successful deconvolution of co-eluting organic compounds. The 2D-chromatographic contours in this study exhibited many peaks in the range of 204-1200 sec (1st dimension) and 1.24-3.25 sec (2nd dimension) for compounds identified in raw and cooling water. Generally, the relatively lower molecular weight compounds also have complexation capabilities with metal cations in natural waters.

Based on the LC-OCD and GC x GC-TOFMS results, the typical NOM fraction in cooling water pipes predominantly contained fulvic acid (Table 2). These results were confirmed by the formation of FEEM spectral contours at excitation/emission wavelengths of 250-450/350-550 nm (Figure 2).

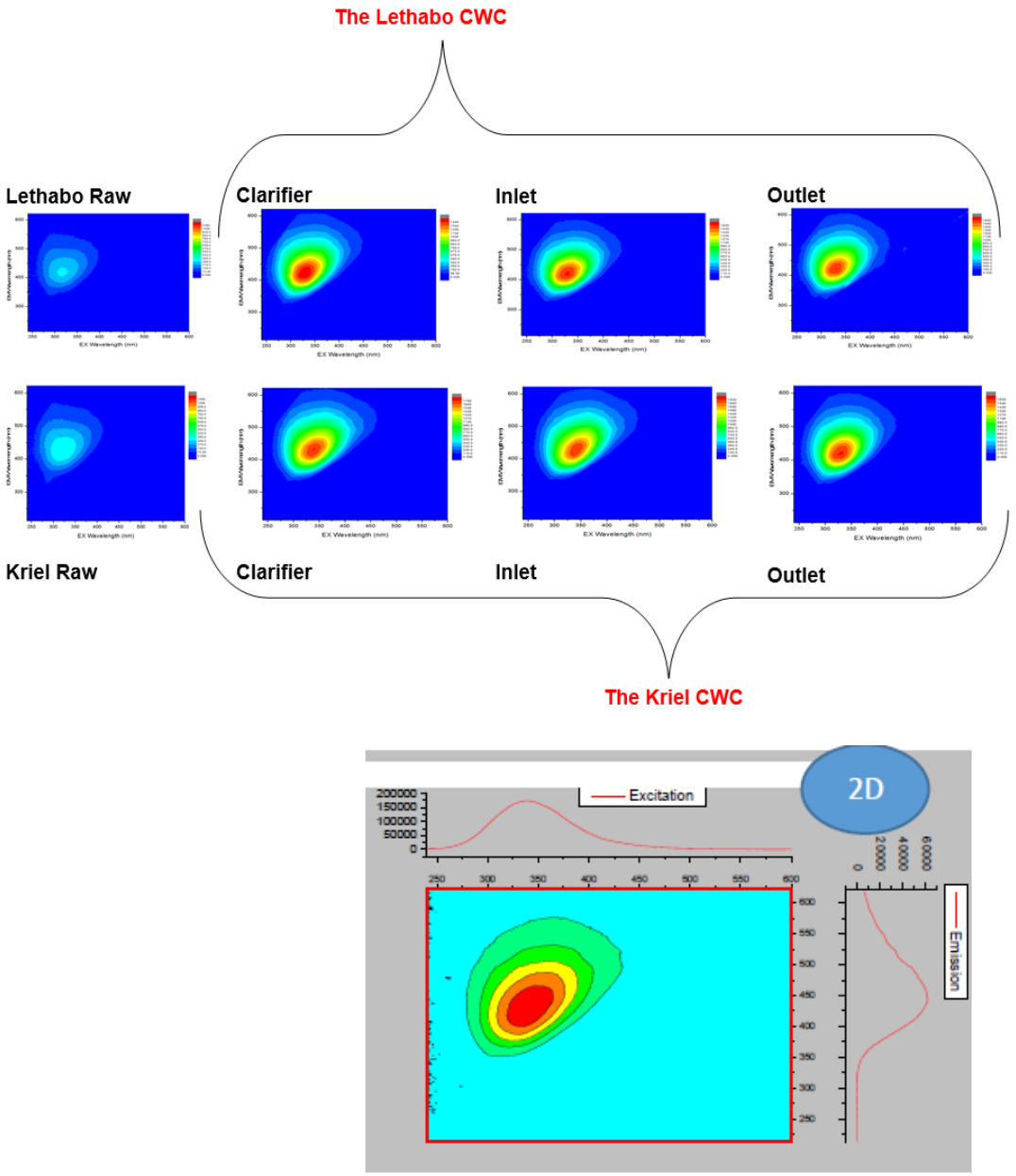

Figure 2: FEEM spectral contours showing the excitation/emission matrices obtained in raw water and water in the CWC at Lethabo and Kriel.

Since the procedure in this study was semi-empirical, the second part of modelling was used to simulate complexation of fulvic acid and scaling cations, alongside some trace metals. Using

the PHREEQC software, the thermodynamic data for phase reactions between fulvic acid and these cations was added into Tipping and Hurley database. That way, successful speciation and saturation index simulations were obtained.

3.3. Modelling computations

There are many databases that can be modified with fulvic acid thermodynamic data. In this work, we focus on the use of the modified Tipping and Hurley-Windermere's humic acid model database (T_H-WHAM database). Specifically, our equilibrium data of metal binding with fulvic acid was obtained from Visual Minteq and incorporated in the T_H-WHAM database. As part of a larger study, the T_H-WHAM has been successfully modified by including equilibrium equations based on Mg, Ca, Zn, Fe, Cu and Ba complexation reactions with the fulvate and humate ion, which were not included in the previous databases. This secondary database, T_H-WHAM, in the PHREEQC code, was then used to generate speciation and saturation index calculations. Differences in the concentration of the complexes formed depended on many factors including the pH, alkalinity, the concentration of anions, the concentration of fulvic acid and the type and concentration of cations in the various stages of the CWC and the concentration of the various metal cations.

The fulvate complexation speciation is shown in Table 4. In these speciation simulations, complex distribution among the metal species were dependent on metal concentrations and the fulvate ion, all obtained experimentally. Besides the concentrations of these species, the pH also influenced complex speciation results. We note that, alkaline conditions were identified in the raw and cooling water samples. The PHREEQC simulation studies at this pH showed that the fulvate ion ranged from 5.54×10^{-6} to 1.08×10^{-6} moles, which showed a tendency to increase with reducing water volumes. However, the concentrations in the various stages in the CWC were within a 10-fold range. A couple of observations were made from the M-fulvate complex simulations (M= Ca, Mg, Ba, Zn and Cu). First, Cu ions bound to more fulvate ions than Zn ions did. Increased trace metal competition for fulvate ions, reduces these anions in water, and consequently increased scaling potentials of the metal ions in CWC pipes. This is so because, scaling potential, also shown by saturation indices (later in this manuscript) is dependent on the amount of ligand available in solution to form stable complexes with Ca and Mg. That way, the free alkaline earth metal ions that would be expected to combine with carbonate/phosphate/silicate/sulphate ions to form insoluble minerals (scale), are reduced. This study showed that the Cu ions reported in this study showed that its presence would compete for the fulvate ions in more less the same way. For instance, the Cu-Fulvate amount was 1.81×10^{-11} and 1.82×10^{-11}, for the raw water obtained from Lethabo and Kriel power stations, respectively. On the other hand, the Ca-fulvate concentrations were 4.627×10^{-13} and 1.058×10^{-12} and Mg-fulvate were 6.743×10^{-12} and 1.187×10^{-11}, for Lethabo and Kriel stations, respectively. Generally, therefore, the Ca/Mg-fulvate concentrations were similar to those of Cu-fulvate but on average, about 10^3 to 10^4-fold more than those of Ba-fulvate and Zn-fulvate. On the extreme, the Fe-fulvate$^+$ were 10^{14} times than those of Ca/Mg/Ba/Cu-fulvate.

Table 5 shows selected mineral phases as a result of experimental inputs (also in Supporting Information Table S4). The Ca/Mg mineral phases that showed scaling tendencies included: Aragonite ($CaCO_3$), artinite ($MgCO_3$: $Mg(OH)_2$:$3H_2O$), brucite ($Mg(OH)_2$), calcite ($CaCO_3$), dolomite ($CaMg(CO_3)_2$), dolomite(d) $CaMg(CO_3)_2$, huntite ($CaMg_3(CO_3)_4$), hydromagnesite ($Mg_5(CO_3)_4(OH)_2$:$4H_2O$) and magnesite ($MgCO_3$). From this study, it is clear that the interaction between calcium and carbonate ions defines scaling to a great extent in water pipes. The saturation indices of aragonite and calcite (polymorphs of $CaCO_3$) are positive throughout the recycle water processes (in raw and in the CWC). These polymorphs remained relatively stable throughout the recycle processes. Many factors that control polymorphic precipitation of these mineral assemblages are reported in the literature. Some of these factors are time

Table 4. Summary of the fulvate complexes in raw and CWCs at Kriel (K) and Lethabo (L) power stations

Complexed species	L-Raw	L-Clarifier	L-inlet	L-outlet	K-Raw	K-Clarifier	K-inlet	K-outlet
Fulvate-2	5.54×10^{-6}	5.64×10^{-5}	3.34×10^{-5}	4.96×10^{-5}	8.07×10^{-6}	6.12×10^{-5}	6.66×10^{-5}	1.08×10^{-4}
HFulvate-	5.27×10^{-11}	6.21×10^{-10}	1.03×10^{-10}	7.40×10^{-10}	1.359×10^{-11}	1.45×10^{-10}	2.973×10^{-11}	2.80×10^{-10}
BaFulvate	1.59×10^{-17}	1.89×10^{-15}	1.38×10^{-15}	2.11×10^{-16}	2.94×10^{-17}	3.32×10^{-16}	5.82×10^{-16}	9.87×10^{-16}
CaFulvate	4.627×10^{-13}	1.541×10^{-11}	9.513×10^{-12}	1.437×10^{-11}	1.058×10^{-12}	7.141×10^{-11}	7.740×10^{-11}	1.341×10^{-10}
MgFulvate	6.743×10^{-12}	6.428×10^{-10}	3.925×10^{-10}	6.062×10^{-10}	1.187×10^{-11}	3.398×10^{-10}	3.819×10^{-10}	6.788×10^{-10}
CuFulvate	1.810×10^{-11}	1.301×10^{-7}	7.802×10^{-9}	2.363×10^{-7}	1.062×10^{-10}	1.718×10^{-8}	1.465×10^{-9}	7.952×10^{-8}
ZnFulvate	4.213×10^{-17}	3.024×10^{-16}	1.013×10^{-16}	5.630×10^{-15}	1.508×10^{-17}	4.326×10^{-16}	5.005×10^{-17}	1.023×10^{-17}
FeFulvate+	1.030×10^{-32}	7.678×10^{-28}	4.562×10^{-28}	2.574×10^{-27}	1.268×10^{-30}	3.155×10^{-30}	4.842×10^{-33}	8.475×10^{-30}

Table 5. Saturation indices of various mineral phases

Mineral	L-Raw	L-Clarifier	L-inlet	L-outlet	K-Raw	K-Clarifier	K-inlet	K-outlet
Anhydrite ($CaSO_4$)	-5.79	-3.67	-3.79	-3.63	-5.25	-3.21	-3.04	-3.24
Antlerite ($Cu_3(OH)_4SO_4$)	-14.53	-8.77	-9.68	-8.35	-13.36	-8.98	-9.24	-7.95
Aragonite ($CaCO_3$)	0.93	0.81	1.17	0.73	0.98	1.84	2.00	1.83
Artinite ($MgCO_3:Mg(OH)_2:3H_2O$)	0.58	-0.31	1.16	-0.63	0.10	0.81	2.45	0.80
Azurite ($Cu_3(OH)_2(CO_3)_2$)	-10.45	-5.36	-6.56	-4.91	-9.42	-5.97	-7.51	-4.87
Barite ($BaSO_4$)	-2.84	-0.17	-1.22	-1.05	-2.39	-1.13	-0.76	-0.96
Bianchite ($ZnSO_4:6H_2O$)	-15.70	-13.24	-13.63	-11.90	-14.96	-13.29	-14.10	-13.22
Brochantite (Cu4(OH)6SO4)	-14.79	-8.38	-9.18	-7.91	-13.52	-8.15	-8.07	-6.79
Brucite ($Mg(OH)_2$)	0.18	-1.04	0.07	-1.28	-0.23	-0.01	1.45	-0.04
Calcite ($CaCO_3$)	1.07	0.96	1.32	0.87	1.12	1.98	2.14	1.97
Chalcanthite ($CuSO_4:5H_2O$)	-17.18	-12.72	-13.86	-12.39	-16.23	-13.81	-14.75	-13.45
CupricFerrite ($CuFe_2O_4$)	11.11	12.69	12.10	13.07	13.58	12.38	11.34	12.79
Cuprite (Cu_2O)	-7.87	-4.23	-5.11	-3.85	-7.16	-4.73	-5.50	-3.97
CuprousFerrite ($CuFeO_2$)	9.31	12.69	10.81	11.95	10.85	10.97	9.90	11.39
Dolomite ($CaMg(CO_3)_2$)	2.84	3.07	3.78	2.90	2.83	4.17	4.51	4.18
Dolomite(d) $CaMg(CO_3)_2$	2.29	2.52	3.23	2.35	2.28	3.62	3.96	3.63
Epsomite ($MgSO_4:7H2O$)	-7.45	-4.87	-5.00	-4.82	-7.02	-5.35	-5.17	-5.35
Goethite ($FeOO_2H_3$)	6.10	6.56	6.22	6.73	7.28	6.19	5.50	6.23
Goslarite I ($ZnSO_4:7H_2O$)	-15.50	-13.05	-13.44	-11.71	-14.77	-13.10	-13.90	-13.03
Gypsum ($CaSO_4:2H_2O$)	-5.57	-3.45	-3.57	-3.41	-5.03	-2.99	-2.82	-3.02

Hematite (Fe_2O_3)	14.21	15.13	14.44	15.47	16.57	14.39	13.01	14.47
Huntite ($CaMg_3(CO_3)_4$)	2.03	2.94	4.36	2.61	1.90	4.20	4.91	4.25
Hydromagnesite ($Mg_5(CO_3)_4(OH)_2:4H_2O$)	-1.5	-1.45	1.08	-2.01	-2.25	-0.09	2.09	-0.05
Jarosite H ($(H_3O)Fe_3(SO_4)_2(OH)_6$)	-32.53	-23.54	-27.06	-22.46	-27.30	-27.69	-32.31	-27.51
Langite ($Cu_4(OH)_6SO_4:H_2O$)	-16.24	-9.83	-10.63	-9.36	-14.97	-9.60	-9.52	-8.24
Maghemite (Fe_2O_3)	3.82	4.74	4.05	5.08	6.17	3.99	2.62	4.08
Magnesite ($MgCO_3$)	1.18	1.53	1.88	1.45	1.12	1.61	1.79	1.63
Magnetite (Fe_3O_4)	10.37	12.92	11.33	13.57	14.15	11.11	8.33	11.29
Malachite ($Cu_2(OH)_2CO_3$)	-5.11	-2.24	-2.78	-1.98	-4.54	-2.32	-2.92	-1.60
Melanterite (FeSO4:7H2O)	-20.50	-15.07	-17.20	-14.47	-18.23	-17.65	-20.33	-17.53
Nesquehonite ($MgCO_3:3H_2O$)	-1.22	-0.88	-0.53	-0.96	-1.28	-0.80	-0.62	-0.78
Portlandite ($Ca(OH)_2$)	-6.34	-8.02	-6.90	-8.27	-6.64	-6.04	-4.60	-6.10
Siderite ($FeCO_3$)	-9.07	-5.88	-7.54	-5.41	-7.29	-7.90	-10.58	-7.75
Siderite(d) ($FeCO_3$)	-9.51	-6.32	-7.98	-5.85	-7.73	-8.34	-11.02	-8.19
Smithsonite ($ZnCO_3$)	-4.72	-4.50	-4.41	-3.28	-4.47	-3.99	-4.79	-3.89
Tenorite (CuO)	-0.83	-0.18	-0.07	-0.13	-0.72	0.26	0.60	0.59
Witherite ($BaCO_3$)	-1.51	-1.07	-1.64	-2.08	-1.55	-1.47	-1.10	-1.28

sequence for the precipitation of calcium, temperature and pH. The results in this study suggest that the pH is responsible for the relative stability of aragonite and calcite. Furthermore, the differences in saturation indices of these two mineral phases do not differ much from each other, between the two power stations.

The Mg mineral phases from the modelling outputs also showed a super saturation/precipitation tendency. However, regardless of the fact that Ca and Mg belong to the same group of elements in the periodic table, Mg carbonate mineral phases showed greater tendencies to precipitate than Ca carbonate minerals (Table 5). The combined Mg and Ca minerals such as dolomite ($CaMg(CO_3)_2$) and dolomite(d) $CaMg(CO_3)_2$, also showed tendencies to scale/precipitate. Most sulphate mineral phases showed high tendencies to dissolve. These included anhydrite ($CaSO_4$), gypsum ($CaSO_4.2H_2O$), antlerite ($Cu_3(OH)_4SO_4$), barite ($BaSO_4$), bianchite ($ZnSO_4:6H_2O$) and Epsomite ($MgSO_4:7H2O$), among others.

No Cu, Ba, Zn or Fe sulphate or carbonate mineral phase was found to precipitate. Nevertheless, hydroxide and oxyhydroxide mineral phases such as cupricFerrite (CuFe2O4) cuprousFerrite (CuFeO2), goethite ($FeOO_2H_3$), hematite (Fe_2O_3), maghemite (Fe_2O_3), magnetite (Fe_3O_4) and tenorite (CuO) were found to have a high tendency to precipitate. Another observation made was the interaction of Fe with various anions and oxidants to form various mineral phases such as cupricFerrite ($CuFe_2O_4$), cuprousFerrite ($CuFeO_2$), goethite ($FeOO_2H_3$), hematite (Fe_2O_3), hydromagnesite ($Mg_5(CO_3)_4(OH)_2:4H_2O$), maghemite (Fe_2O_3) and magnetite (Fe_3O_4). All these mineral phases were found to be highly precipitating. In the current state, iron binding to fulvic acid is minimal compared to other metals. For instance, the molality values of FeHumate+ are extremely low viz; 1.030×10^{-32}, 7.678×10^{-28}, 4.562×10^{-30} and 2.574×10^{-27} in raw clarified, inlet and outlet stages in the cooling water process. These values are 10^10 fold the complexation values of the other metals. On the contrary, literature suggests that Fe is highly complexing to organic ligands. This calls for further research. The manipulation of physicochemical parameters that inhibit its complexation of the metals to humic substances, in favour of Ca, while reducing the components that oxidise, will probably explain this scenario.

Given the results in Tables 4 and Table 5, we can conclude that the complexation studies between cations and humates/fulvates could be linked to saturation indices in explaining the scaling potential. Saturation index results show that only the values in raw water samples are slightly different. However, the fact is that the incorporation of the equilibrium equations for Ba, Ca, Fe, Mg, Cu and Zn with humates/ fulvates into the PHREEQC databases, could offer a special link that explains simultaneous complexation and precipitation reactions in fresh waters used for industrial purposes.

3.4. Applicability of experimental and modelling studies to scaling control

The PHREEQC model simulations have been previously described and typical examples given [35]. PHREEQC applications have been demonstrated to provide useful outputs on elemental speciation and their saturation indices in aqueous media, the quality of input information from empirical studies notwithstanding. Any changes in experimental inputs into the PHREEQC code will change the simulated distribution of resultant species in water. In this article, the composition of scale in pipes, physico-chemical conditions determined, are given in Table 6. The experimental results shown in Table 6 were obtained from analysis of a scale sample obtained from cooling water pipes. They showed varied concentrations of elements in the order of Si>Mg>Cu>Al>Zn>Fe>Ca>F>S>Sn.

The other step is to accurately determine the content of scaling metals and other trace elements in water. The fundamental objective here is to keep these ions in complexed solution form.

Therefore, it was important to include organic compounds in the PHREEQC databases and simulate scale formation under different conditions (shown in the methodology section). A typical illustration of precipitative and complexation discussion has been discussed using fulvic acid interactions with metal cations.

Table 6. The XRF results of the components of scale obtained from Lethabo cooling water pipes

Phase name	Formula	% by mass
Smithsonite	$Zn(CO_3)$	0.4
Zinc Phosphate	$Zn(PO_3)_2$	28.3
Zinkosite, syn	$ZnSO_4$	19.8
Calcium iron(II) oxide	$CaFeO_2$	5.5
Berlinite; berlinite, syn	$Al(PO_4)$	35.6
Magnesite, syn	$Mg\ (CO_3)$	0.5
Calcium Silicide	$CaSi_2$	0.3
Aragonite	$Ca\ (CO_3)$	7.5
Dolomite	$Ca\ Mg\ (CO_3)_2$	0.2
Diaspore, syn	AlO(OH)	1.3
Gypsum	$CaSO_4 \cdot 2H_2O$	0.6

The temperatures under which cooling towers normally operate, leads to evaporation of cooling water in the open circuit. For this reason, it important to determine accurately the organics and metals in water before modelling. However, identifying and measuring the organic compounds in water is cumbersome. Since the organic compounds have been collectively as natural organic matter, it would be necessary to characterize the main components in water. The results in this study, showed that by using the LC-OCD, GC x GC-TOFMS and FEEM, important information on NOM in water would be obtained. This characterization effort in this study showed that NOM in water is made up of humic substances, predominantly fulvic acid. Additional information confirming the identity and quantity of fulvic acid is shown in Figure 2, Table 7 and Figure 3. The results mapped out on the HS-diagram, show that the composition of NOM falls predominantly on the fulvic region. Additionally, an evaporation (in an open system), shows that the fulvic acid concentrations increased with reducing volumes (considered to reduce with time). Briefly, these changes are described as follows.

For practical purposes water recycling at Eskom results into highly saline (with high levels of total dissolved species) water. This high concentration of total dissolved solids (TDS) could result in enhanced scaling in power plant pipes. In this case, the main usefulness of the saturation index to indicate the likelihood of precipitation of calcium carbonate and other ions in the must be described vis-à-vis complexation. As the cations and inorganic compounds concentrate, the organic compounds change in form, and probably concentrate too. Using the LC-OCD-OND, the organic compounds can be characterised and quantified (Table 7). This is an important step that can help to monitor the changes in organic matter. Additionally, a known quantity of raw and cooling water samples, was evaporated at 45 ˚C and samples analysed progressively for the organics to verify the changes in the distribution of organic compounds. The results of this simulation are presented in Table 7 and the corresponding mapping on the HS-diagram (Figure 3). A scan through the HS-diagram shows that the molecular weight reduces with time. This was in close agreement with the SUVA values. The specific UV absorbance at λ_{254} and the HS-diagrams show the relationship between aromaticity and molecular weights of various compounds.

This series of measurements provided inputs for model codes. The model PHREEQC code in this study, allowed for the determination of the species at the observed pH conditions, while

also proving that the resultant saturation indices give a picture of the components of scale (Table 6) at the given water conditions and constituents. This is a key point in obtaining reproducible speciation information, which verifies experimental data. This study, on metal-fulvate speciation, as a function of pH values, and their concentrations, was performed to show the scaling potential in each stage of the cooling water process. It is worth noting that the metal-fulvate complexation trends can be predicted by equilibrium calculations if the log k values for the complexation reaction in equilibrium is known.

Table 7. NOM fractions. (DOC=dissolved organic carbon, BP=biopolymers, HS=humic substances, SUVA=specific ultra-violet absorbance, BBs=building blocks, LMWN=Low molecular weight (MWt) neutrals, LMWA=Low MWt acids)

	DOC	BP	(HS)	(Norg)	(SUVA-HS)	(MWt)	HS diagram	BBs	LMWN	LMWA
	ppm-C	% DOC	% DOC	ppm-N	L/(mg*m)	g/mol	--	% DOC	% DOC	% DOC
RW	7.47	2.7	59.2	0.24	3.5	477	A	1.1	1.3	n.q.
CW	48.5	8.1	56.8	1.1	2.7	467	B	1.5	1.5	n.q.
CW 28	98.3	7.6	57.8	2.1	2.9	401	C	1.5	1.1	0.05
CW 42	113.6	4	58.9	3	2.8	395	D	1.7	1.2	0.001
CW 56	138.9	4.6	59.4	4.6	2.9	402	E	1.9	1.2	n.q.
CW 73	199	4.4	58.6	6.5	2.9	386	F	1.9	1.2	n.q.
R 29	109	2.1	48.8	0.25	4	450	G	1.3	2.6	n.q.
R 45	135	1.9	47.4	0.34	3.9	459	H	1.4	2.6	n.q.
R 56	162.7	1.9	48.1	0.45	3.9	427	I	1.3	2.9	n.q.
R 70	182.6	1.9	48.4	0.48	3.9	420	J	1.2	2.8	n.q.

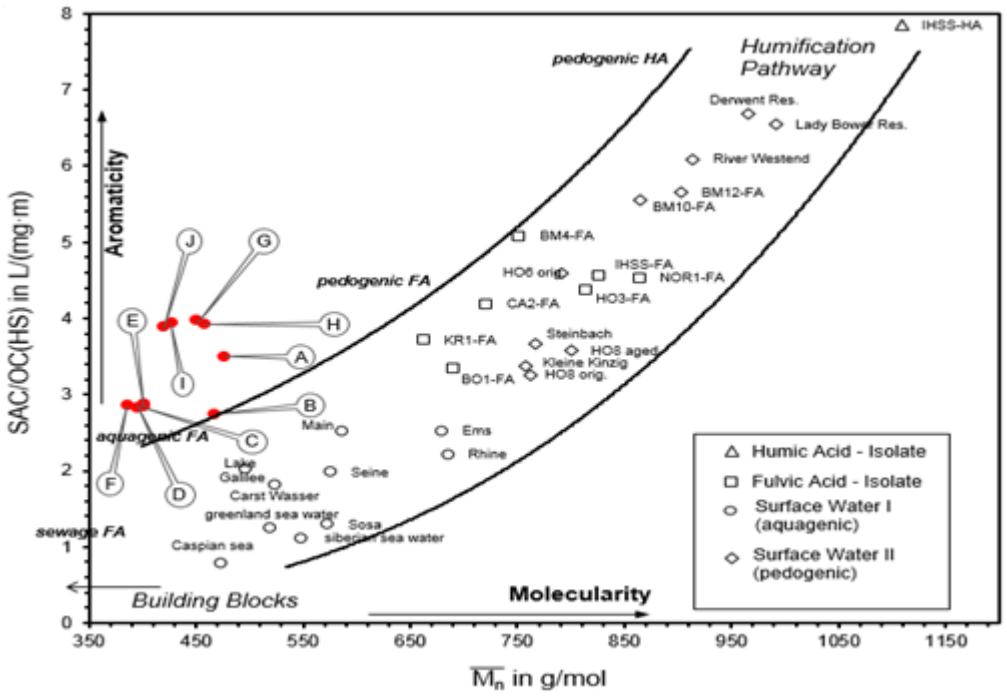

Figure 3: The HS-diagram of raw, CW and simulated evaporation water samples (A to H are shown in Table 7)

Future work will concentrate on the how the various NOM fractions are distributed in allochthonous and autochthonous NOM. From our study, the biopolymers and humic substances (organics of high molecular weights i.e. 20,000–100,000 g/mol and approximately 1000 g/mol, respectively), can be categorized very well using LC-OCD. The fulvate predominance in the water throughout the stages (shown by the HS-diagram) were included in

databases and modelled. Using a modified T_H_WHAM.DAT new complexation outputs were generated by the PHREEQC code. This entire study has shown that if the concentrations of organics (such as fulvic acid) are known, Ca/Mg complexation favouring conditions with organics could be manipulated and henceforth the control of the incidence and minimizes the magnitude of scaling.

4. Conclusions

Elemental speciation experiments to account for complexation with DOM are few, and the majority of those in the literature, do not account for complexation as a function of scaling in pipes in natural water conditions. In this study, a semi-empirical approach encompassing empirical laboratory measurements and computer based modelling (PHREEQC), yielded valuable knowledge on DOM-metal complexation (Mg, Ca, Cu, Ba, Zn and Fe) and their scaling potentials. The experimental results were successfully obtained by the LC-OCD, GC x GC-TOFMS and FEEM. Modelling results suggest that Ca, Mg, Cu and Fe-based mineral phases had high potential to precipitate. Therefore, the formation of fulvate species with these metals could affect the extent of scaling.

Acknowledgements

The authors of this paper are grateful to the Centre for Nanomaterials Science Research and the Faculty of Science which hosts the Department of Applied Chemistry at the University of Johannesburg. Many thanks to David Parkhurst of the USGS for providing the authors with valuable information.

References

[1] J.S. Gaffney, N.A. Marley and S.B. Clark, Humic and fulvic acids: isolation, structure, and environmental role, Proceedings of a symposium at the 210th American Chemical Society's National Meeting, Chicago, Illinois, USA, August 1995.

[2] E. Tipping, Cation binding by humic substances, Cambridge University Press, 2002.

[3] R. Vidali, E. Remoundaki and M. Tsezos, An experimental and modeling study of humic acid concentration effect on H+ binding: Application of the NICA-Donnan model, Journal of Colloid and Interface Science, vol 339, pp. 330-335, 2009.

[4] A. Iglesias, R. Lopez, S. Fiol, J. Antelo and F. Arce, Analysis of copper and calcium–fulvic acid complexation and competition effects, Water research, vol 37, pp. 3749-3755, 2003.

[5] Y. Lu and H.E. Allen, Characterization of copper complexation with natural dissolved organic matter (DOM)-link to acidic moieties of DOM and competition by Ca and Mg, Water research, vol 36, pp. 5083-5101, 2002.

[6] T. Cheng and H.E. Allen, Comparison of zinc complexation properties of dissolved natural organic matter from different surface waters, Journal of environmental management, vol 80, pp. 222-229, 2006.

[7] P. Zhou, H. Yan and B. Gu, Competitive complexation of metal ions with humic substances, Chemosphere, vol 58, pp. 1327-1337, 2005.

[8] K.G. Mostofa, C.Q. Liu, X. Feng, T. Yoshioka, D. Vione, X. Pan and F. Wu, Complexation of Dissolved Organic Matter with Trace Metal Ions in Natural Waters, in: K.M.G. Mostofa, T. Yoshioka, A. Mottaleb, D. Vione (Eds.), Photobiogeochemistry of Organic Matter, Springer Berlin Heidelberg, pp. 769-849, 2013.

[9] J. Guthrie, N. Hassan, M. Salam, I. Fasfous, C. Murimboh, J. Murimboh, C. Chakrabarti and D. Grégoire, Complexation of Ni, Cu, Zn, and Cd by DOC in some metal-impacted freshwater lakes: a comparison of approaches using electrochemical determination of free-metal-ion and labile

complexes and a computer speciation model, WHAM V and VI, Analytica Chimica Acta, vol 528, pp. 205-218, 2005.

[10] M. Klučáková, M. Pekař, Behaviour of partially soluble humic acids in aqueous suspension, Colloids and Surfaces A: Physicochemical and Engineering Aspects, vol 318, pp. 106-110, 2008.

[11] R. Marsac, M. Davranche, G. Gruau, A. Dia, M. Pédrot, M. Le Coz-Bouhnik and N. Briant, Effects of Fe competition on REE binding to humic acid: Origin of REE pattern variability in organic waters, Chemical Geology, vol 342, pp. 119-127, 2013.

[12] N. Adegboyega, V.K. Sharma, K. Siskova, R. Zboril, M.L. Sohn, B.J. Schultz and S. Banerjee, Interactions of Aqueous Ag+ with Fulvic Acids: Mechanisms of Silver Nanoparticle Formation and Investigation of Stability, Environmental Science & Technology, vol 47(2), pp. 757-764, 2012.

[13] I. Christl, Ionic strength-and pH-dependence of calcium binding by terrestrial humic acids, Environmental Chemistry, vol 9, pp. 89-96, 2012.

[14] D.G. Kinniburgh, C.J. Milne, M.F. Benedetti, J.P. Pinheiro, J. Filius, L.K. Koopal and W.H. Van Riemsdijk, Metal ion binding by humic acid: application of the NICA-Donnan model, Environmental Science & Technology, vol 30, pp. 1687-1698, 1996.

[15] J. Ritchie and E. Perdue, Proton-binding study of standard and reference fulvic acids, humic acids, and natural organic matter, Geochimica et Cosmochimica Acta, vol 67, pp. 85-96, 2003.

[16] S.A. Huber, A. Balz, M. Abert and W. Pronk, Characterisation of aquatic humic and non-humic matter with size-exclusion chromatography–organic carbon detection–organic nitrogen detection (LC-OCD-OND), Water research, vol 45, pp. 879-885, 2011.

[17] A. Batsch, D. Tyszler, A. Brügger, S. Panglisch and T. Melin, Foulant analysis of modified and unmodified membranes for water and wastewater treatment with LC-OCD, Desalination, vol 178, pp. 63-72, 2005.

[18] T. Faludi, A. Vasanits-Zsigrai, G. Záray and I. Molnár-Perl, Identification, quantification and distribution of substituted phenols in the dissolved and suspended phases of water samples by gas chromatography tandem mass spectrometry: Derivatization, mass fragmentation and acquisition studies, Microchemical Journal, vol 118, pp. 45-54, 2015.

[19] N. Fontanals, R.M. Marcé and F. Borrull, New materials in sorptive extraction techniques for polar compounds, Journal of Chromatography A, vol 1152, pp. 14-31, 2007.

[20] J. Chen, E.J. LeBoeuf, S. Dai and B. Gu, Fluorescence spectroscopic studies of natural organic matter fractions, Chemosphere, vol 50, pp. 639-647, 2003.

[21] J.B. Fellman, E. Hood and R.G.M. Spencer, Fluorescence spectroscopy opens new windows into dissolved organic matter dynamics in freshwater ecosystems: A review, Limnology and Oceanography, vol 55, pp. 2452-2462, 2010.

[22] G.J. Hall, K.E. Clow and J.E. Kenny, Estuarial fingerprinting through multidimensional fluorescence and multivariate analysis, Environmental science & technology, vol 39, pp. 7560-7567, 2005.

[23] S.R. Charlton and D.L. Parkhurst, Modules based on the geochemical model PHREEQC for use in scripting and programming languages, Computers & Geosciences, vol 37, pp. 1653-1663, 2011.

[24] A. Nardi, A. Idiart, P. Trinchero, L.M. de Vries and J. Molinero, Interface COMSOL-PHREEQC (iCP), an efficient numerical framework for the solution of coupled multiphysics and geochemistry, Computers & Geosciences, vol 69, pp.10-21, 2014.

[25] D. Parkhurst and C. Appelo, Description of input and examples for PHREEQC version 3: a computer program for speciation, batch-reaction, one-dimensional transport, and inverse geochemical calculations, US Geological Survey, 2013.

[26] D.L. Parkhurst and C.A.J. Appelo, PHREEQC Interactive, United States Geological Survey, Denver, version 2 (2007).

[27] S.E. Cabaniss, Forward modeling of metal complexation by NOM: I. A priori prediction of conditional constants and speciation, Environmental Science & Technology, vol 43, pp. 2838-2844, 2009.

[28] S.E. Cabaniss, Forward modeling of metal complexation by NOM: II. Prediction of binding site properties, Environmental Science & Technology, vol 45, pp. 3202-3209, 2010.

[29] J.P. Gustafsson, Modeling the acid–base properties and metal complexation of humic substances with the Stockholm Humic Model, Journal of Colloid and Interface Science, vol 244, pp. 102-112, 2011.

[30] O. Pourret, M. Davranche, G. Gruau and A. Dia, Organic complexation of rare earth elements in natural waters: evaluating model calculations from ultrafiltration data, Geochimica et Cosmochimica Acta, vol 71, pp. 2718-2735, 2007.

[31] G.O. Bosire, J.C. Ngila and J.M. Mbugua, Predictive complexation models of the impact of natural organic matter and cations on scaling in cooling water pipes: a case study of power generation plants in South Africa, Physics and Chemistry of the Earth, Parts A/B/C, Vol 76–78, pp. 35-41 2015.

[32] K. Warnken, W. Davison, H. Zhang, J. Galceran and J. Puy, In situ measurements of metal complex exchange kinetics in freshwater, Environmental Science & Technology, vol 41, pp. 3179-3185, 2007.

[33] W. Chen, P. Westerhoff, J. Leenheer and K. Booksh, Fluorescence Excitation−Emission Matrix Regional Integration to Quantify Spectra for Dissolved Organic Matter, Environmental Science & Technology, vol 37, pp. 5701-5710, 2003.

[34] V. Pather, Eskom and water, Proceedings of the 2004 Water Institute of Southern Africa (WISA) Biennial Conference, Cape Town, South Africa, 2004. URL: http://www. ewisa. co. za/literature/files/260. pdf (Accessed October 2010).

[35] D.L. Parkhurst and C. Appelo, Description of input and examples for PHREEQC version 3 - A computer program for speciation, batch-reaction, one-dimensional transport, and inverse geochemical calculations, 2013.

Biographical information

Dr Bosire obtained his PhD in Analytical/Inorganic and Computational Chemistry from the University of Johannesburg, South Africa. Dr Bosire is skilled in data modelling using computer codes and comfortable with manipulation of different software including the Discovery Studio, *Materials Studio,* Spartan, R, Python, SOLO, SOLO+MIA, MINEQL+, MINTEQA2, Visual MINTEQ, PHREEQC, GeoChemist's WorkBench and STATA, all applicable in nanotechnology (Material Science and Drug Discovery) and semi-empirical studies in Chemistry.

Professor Ngila obtained her PhD in Analytical-Environmental chemistry from the University of New South Wales in Australia. She has elaborate experience in water and oil research, chemical resins, adsorbents and nanotechnological advances. She has received many awards to her name including the recent African Union Kwame Nkrumah Award for Scientific Excellence (2016). Currently,

Prof Ngila is a Full Professor at the Johannesburg and the Deputy Director, Training, Academic & Linkages, at the Morendat Institute of Oil & Gas (MIOG), Kenya Pipeline Company.